Ultrasonics 54 (2014) 2141–2150

Contents lists available at ScienceDirect

Ultrasonics

journal homepage: www.elsevier.com/locate/ultras

Ultrasound generation with high power and coil only EMAT concepts

Dirk Rueter *, Tino Morgenstern

University of Applied Sciences Ruhr West, 45473 Muelheim, Germany

ARTICLE INFO

Article history:
Received 12 February 2014
Received in revised form 22 May 2014
Accepted 17 June 2014
Available online 3 July 2014

Keywords:
EMAT
Pulsed power
Non-linear effects
Spark induced ultrasound
Laser induced ultrasound

ABSTRACT

Electro-magnetic acoustic transducers (EMATs) are intended as non-contact and non-destructive ultrasound transducers for metallic material. The transmitted intensities from EMATS are modest, particularly at notable lift off distances. Some time ago a concept for a "coil only EMAT" was presented, without static magnetic field. In this contribution, such compact "coil only EMATs" with effective areas of 1–5 cm^2 were driven to excessive power levels at MHz frequencies, using pulsed power technologies. RF induction currents of 10 kA and tens of Megawatts are applied. With increasing power the electroacoustic conversion efficiency also increases. The total effect is of second order or quadratic, therefore non-linear and progressive, and yields strong ultrasound signals up to kW/cm^2 at MHz frequencies in the metal. Even at considerable lift off distances (cm) the ultrasound can be readily detected. Test materials are aluminum, ferromagnetic steel and stainless steel (non-ferromagnetic). Thereby, most metal types are represented. The technique is compared experimentally with other non-contact methods: laser pulse induced ultrasound and spark induced ultrasound, both damaging to the test object's surface. At small lift off distances, the intensity from this EMAT concept clearly outperforms the laser pulses or heavy spark impacts.

© 2014 The Authors. Published by Elsevier B.V. This is an open access article under the CC BY-NC-ND license (http://creativecommons.org/licenses/by-nc-nd/3.0/).

1. Introduction

Conventional electromagnetic acoustical transducers (EMATs) include a permanent magnet and an induction coil. The coil induces RF eddy currents into a metallic test object. The RF eddy currents and the presence of the permanent field B_0 result in oscillating Lorentz forces, i.e., ultrasound excitation in the metal. The method excites metallic test objects over some distance via immaterial magnetic fields. As an appreciated feature, this magnetic ultrasound transduction readily permeates most non-metallic barriers (air, oxides, oil, painting, humidity, packaging material: paper, plastic foil, etc.). A variety of possible geometries and ultrasound modes (shear waves, longitudinal waves, etc.) can be applied. As a fundamental problem, the transmitted ultrasound intensities from EMATs are modest. Usually, only very small "lift off" distances in the range of less than few mm are practical for proper EMAT operation. On the other hand, many application fields – like heavy steel industries or prepackaged metal parts – would appreciate increased lift off distances or higher ultrasound intensities for crude and large test objects. Additionally, permanent magnetic fields from conventional EMATs attract ferromagnetic particles. Such adhering particles potentially disturb the measurement or even may cause mechanical damage to the transducer or the test object. Some recent EMAT types utilize pulsed electromagnets for B_0, thereby avoiding that problem (Refs. [1–4]).

In this contribution "coil only EMATs" are investigated, i.e., a permanent magnetic field is lacking. Instead, the RF induction field itself interacts with excited (and orthogonal) eddy currents in the test object, producing Lorentz forces and acoustic pressure in the sample. This concept was already investigated by Jian et al. (Refs. [5,6]). The authors modeled and experimentally verified (Ref. [5]) the ultrasound emission from two different EMAT systems (spiral coil and line coil). Lorentz forces and displacements in the test metal resulted from eddy current and a permanent (static) field B_0 and additionally – of particular interest here – from eddy current and the RF induction field itself (i.e., the dynamic field). With 0.1 mm lift-off, a static field $B_0 = 0.395$ T and a characteristic excitation frequency around 300 kHz the authors found (cited literally from Ref. [5]) "the force due to the dynamic field is about five times larger than the Lorentz force due to the applied static magnetic of 0.395 T". This remark is very interesting, since the permanent field B_0 in conventional EMATs cannot be easily increased by a factor of five: for Ref. [5] this would be a quite challenging 2 T and that is currently not possible with conventional magnet materials.

EMAT schemes without a static field were also mentioned in even older textbooks (e.g., Ref. [7]). Herein, the occurring Lorentz forces are recognized to be exclusively repulsive, they increase with the square of excitation current and they oscillate with a

* Corresponding author. Tel.: +49 1606321020.
E-mail addresses: dirk.rueter@hs-ruhrwest.de (D. Rueter), Tino.morgenstern@hs-ruhrwest.de (T. Morgenstern).

http://dx.doi.org/10.1016/j.ultras.2014.06.012
0041-624X/© 2014 The Authors. Published by Elsevier B.V.
This is an open access article under the CC BY-NC-ND license (http://creativecommons.org/licenses/by-nc-nd/3.0/).

doubled frequency. For relatively low frequencies (100 kHz...) considerable ultrasound intensities (at doubled frequency) were quoted, although not explicitly quantified. The lacking permanent magnet allows more compact and robust designs (e.g., no critical temperature limits of certain magnetic materials). As a clear disadvantage (Ref. [6,7]), without a static field this EMAT scheme cannot readily detect ultrasound, it then exclusively works as a transmitter. Possible ways to overcome this inherent obstacle are discussed below in the conclusions.

Additionally, a good understanding and much experience about strong Lorentz forces and high pressures from "coil only transducers" already has existed for decades in the well-established field of electromagnetic forming (EMF) (Ref. [8]). In EMF not only pressures onto a metal are generated over a distance ("non-contact") via pulsed magnetic fields. Additionally, these forces are strong enough to overcome the structural strength of the work piece. Then the metal gives way to the pressure pulse and undergoes a rapid and considerable deformation. EMF is industrially exploited as a non-contact tool for joining and forming metallic work pieces (Refs. [9–11]). The characteristic frequency range of a pulse for EMF is in the order of just 10 kHz, corresponding to several tens of µs for a single half wave. These kHz frequencies are chosen to optimize the overall EMF process and its efficiency. The generation of ultrasound is not intended in EMF, although recognized as a by-product. The very strong Lorentz forces in EMF – readily beyond limits for non-destructive testing (NDT) – encourage the consideration of this principle for intense and non-contact ultrasound generation.

Our intention is the investigation of powerful and magnetically induced (non-contact) ultrasound at notably higher frequencies (i.e., >1 MHz instead of 300 kHz or less), suitable for NDT. Furthermore, increased lift off distances towards 1 cm instead of just 1 mm or less are approached, interesting for more or new application fields like prepackaged products. The underlying physics is viewed under the terminology *magnetic pressure* (more common in EMF technologies) instead of explicitly evaluating eddy currents and Lorentz forces (as typically done in EMAT considerations). The approach via magnetic pressure appears to be more convenient here and it still reasonably describes the actual findings from experiments.

The well-known fundamentals of EMF also apply at MHz frequencies and can be briefly explained by Figs. 1–3 and some robust relations. For EMF technology, such relations and approximations are found to sufficiently match the experimental observations and in addition, they are quite lucid and handy (Ref. [11]). Due to the complex geometries of magnetic fields and eddy currents in EMAT geometries, an analytically exact description can just be

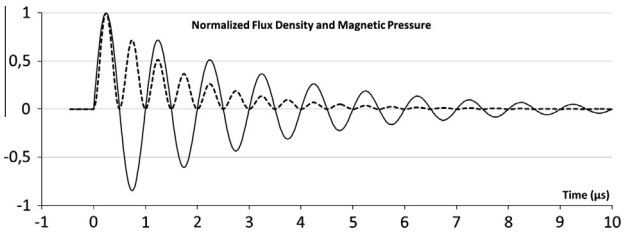

Fig. 2. At 0 µs a damped 1 MHz oscillation (solid line) of the magnetic flux density B is started. The energy density or magnetic pressure is proportional to B^2 and is displayed by the interrupted line. The pressure exclusively obtains positive polarity and it oscillates at 2 MHz. Idealized and normalized representation from a calculation, $\tau = 3$ µs.

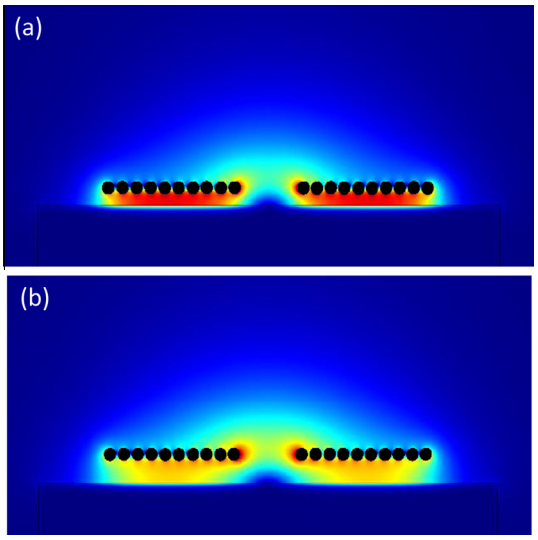

Fig. 3. Magnetic field intensity in intuitive colors from a flat spiral coil at $g = 1$ mm (Fig. 3a) and at $f = 1$ MHz, over a highly conductive copper block (lower rectangle). Cross sectional view similar to Fig. 1c. The B field virtually cannot permeate into the metal but is shielded (or compensated) by eddy currents. Therefore the field is concentrated in the gap g, the field direction is radial and parallel to the metal surface (not visualized here). In Fig 3b the gap g is doubled to 2 mm and the current in the coil is unchanged. Now the field intensity in the gap is notably decreased and the field tends to localize around the coil. Images generated from simulation.

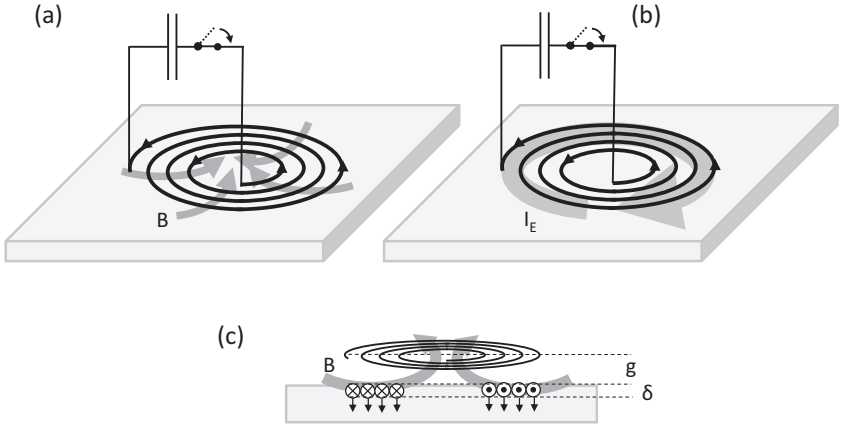

Fig. 1. A capacitor discharges into a flat spiral coil. The coil is positioned close to a metallic test object. The released energy converts into a magnetic field B, this field is directed radially and parallel to the metallic surface (a). A contra-directional eddy current I_E is induced in the metal beneath the coil (b). The magnetic field B and the eddy current are restricted to the skin depth δ and result into Lorentz forces or a pressure normally into the depth of the metal (c). The effect works over some distance g.

derived for simple geometries (such as a current line or a current loop parallel over a metallic plane). Due to a more extensive and abstract evolution this way is not approached in this practically motivated contribution. Instead, the problem is modeled in a FEM computation (as also carried out in Ref. [5]). The FEM modeling yields a numerical correction for some quite basal approximations and finally, with this correction, the experimental values are found in reasonable accordance:

A capacitor C is charged to high voltage levels U. The stored energy E in the capacitor is (Eq. (1a))

$$E = \frac{1}{2} C \cdot U^2 \tag{1a}$$

and

$$E = \frac{1}{2} L \cdot I_{el}^2 \tag{1b}$$

In commercially available EMF machines E reaches or even considerably exceeds 10 kJ. After closing a switch (Fig. 1), the capacitor C will rapidly (in EMF: within 10^{-5}–10^{-4} s) discharge into an inductor L. Such an inductor L can be realized as a flat spiral coil. For ideal elements (switch, L and C) the stored energy E is fully converted into a magnetic field of the inductor L with discharge current I_{el}, described by Eq. (1b). The arrangement represents a simple L-C-oscillation circuit; the current in the conductor (and the associated magnetic field) then will oscillate with a characteristic frequency f. The characteristic electrical impedance Z_{el} is the ratio of voltage amplitude and current amplitude in the oscillating L-C-circuit:

$$f = \frac{1}{2\pi\sqrt{L \cdot C}} \tag{2a}$$

$$Z_{el} = \sqrt{\frac{L}{C}} \tag{2b}$$

For NDT ultrasound, L-C-frequencies in the order of 10^6 Hz are interesting and this can be readily achieved by choosing elements L and C with relatively smaller values. The available maximum electrical power $P_{el,max}$ from such oscillating L-C-circuit is

$$P_{el,max} = \frac{1}{4} \cdot \frac{U^2}{Z_{el}} = \frac{1}{4} \cdot \frac{1}{\sqrt{L \cdot C}} \cdot C \cdot U^2 = \pi \cdot f \cdot E \tag{3}$$

When extracting this available maximum power (Eq. (3)) from the L-C-circuit, the oscillating energy (Eq. 1) will essentially be consumed in less than a single half-wave. $P_{el,max}$ is used below as a reference power for efficiency considerations.

In practical setups, neither the coil nor the switch nor the capacitor is ideal. The energy losses and resistance of these elements result into a damped oscillation of the current or the magnetic flux density B

$$B(t) \sim \sin(2\pi f t) \cdot e^{-\frac{t}{\tau}} \tag{4}$$

where $\tau = L/R$ and R is an equivalent serial resistance in the L-C-circuit to represent energy losses after closing the switch. Fig. 2 displays a damped 1 MHz oscillation with $\tau = 3$ µs.

When positioning a flat spiral coil L close to a metallic object in a distance g (the lift off gap), the magnetic field B has a mainly radial component parallel to the metal surface. The oscillating field will induce an annular and contra-directional eddy current in the metal below the spiral (Fig. 1a and b). This eddy current couples back to the spiral coil and affects the frequency f (usually increases) and the decay time τ (usually decreases) of the L-C-circuit. Particularly at very close coupling between inductor and metal noticeable changes result. The general L-C-behavior however, is not principally affected at moderate coupling, and for the sake of clarity these effects are not explored in more detail here, see instead a focused elaboration in Ref. [6].

It is well known that an RF eddy current is carried by just a thin surface layer of the metal, with effective thickness δ ("skin", skin effect) (see e.g. Ref. [12]). At 1 MHz, the characteristic thickness δ is about 85 µm for aluminum, about 400 µm for (non-ferromagnetic) stainless steel and for ferromagnetic steel about 10 µm (if magnetic flux density below saturation, up to 1.5 T) or about 200 µm (flux density above 2 T) (Ref. [12]). Neither the eddy current nor the RF magnetic field can permeate the metal much deeper than the skin depth δ: the induced and contra-directional eddy current itself generates a magnetic field. That additional field finally eliminates (subtracts) all resulting magnetic field below the skin depth. It increases (adds, direction reversed) the resulting magnetic field *above* the surface, within the lift off gap. Furthermore, *above* the excitation coil (here the excitation field is reversed) the eddy current again weakens the field. Therefore, the resulting magnetic field B at RF frequencies and in an arrangement according to Fig. 1 is practically forced above and parallel to a metal surface, and in addition, the highest flux densities are present in the lift off gap g.

It should be noted that for a given RF magnetic field the total eddy current is – even for different metal types with different conductivity – virtually the same. This behavior implicitly results from the compensation – by eddy currents – of all induction fields in the volume of a metal. Fig. 3 illustrates a FEM simulation for a magnetic flux density. The computed scenario displays the cross section of a "flat spiral coil with RF excitation above a metallic surface". The intensity of B is intuitively represented by the color. Near the metal, the B field is directed parallel to the surface, the direction itself is not visible in this presentation. The B field does virtually not permeate the metal; it is restricted to the relatively thin surface layer δ. In the gap g between metal and coil the field appears relatively strong and (particularly for Fig. 3a) fairly homogeneous. Above the coil the field is much weaker; the field is not symmetric with respect to the coil plane. For different kinds of metal (different skin depth δ) the general appearance of Fig. 3 does virtually not change, as long as the gap g between coil and metal is significantly higher than skin depth δ (which is implied in this simulation).

As a further remark, the virtually equal eddy currents for quite different types of metals (good conductivity vs. poor conductivity) do not imply an equal energy consumption from the excitation coil: The phase between voltage and current of the inductor system is shifted below 90° by imperfect conductors (either caused by the imperfect coil itself or by the inductively coupled target metal), thus increasing the effective serial resistance R and reducing the τ (Eq. (4)). Actually, a reduced τ *for* a target metal with relatively poor conductivity – here stainless steel – is experimentally observed below.

When comparing the modeling of Fig. 3a and b (same excitation current implied), the field in the smaller gap of Fig. 3a appears to be more concentrated and more homogeneous. In addition, the residual field *above* the coil plane is weaker than in Fig. 3b. The field intensity around the coil is considerably deformed by the superimposing field from the eddy current. When numerically integrating the magnetic energy density (being proportional to B^2, see from Eq. (5) below) over the volume in the FEM models, for Fig. 3a about 69% of the total magnetic field energy is accumulated in the volume below the coil center plane. Actually it is concentrated between the coil windings and the metal surface. For the scenario with the increased gap (Fig. 3b) the relative energy content in the gap accounts to a somewhat less 65%, relatively more field energy is then also present above the coil, apart from the target.

As a reasonable approximation – derived from such FEM data (Fig. 3a and b) and as usually done in EMF techniques – it can be stated, that in a scenario where the gap g is smaller than 1/10 of the active radius of a flat spiral coil, the magnetic energy of the system (Eq. (1b)) will predominantly (i.e., >70%) be present in the gap.

The annular eddy current and the mostly radial magnetic field – both parallel to the metal surface – result into Lorentz forces. These distributed forces are directed normally into the depth (Fig. 1c) and are experienced as a pressure p. As an important detail, this pressure is also positive for a negative half wave of the oscillating magnetic field (Fig. 2 and Refs. [5,7]). Not only the B field but also the accompanying eddy current periodically changes the polarity, only positive pressure is produced (as intended in EMF). As an inherent consequence the Lorentz forces or pressure then will then oscillate at a doubled frequency (Ref. [7]). Furthermore, the Lorentz force is proportional to the magnetic flux density B and the eddy current, which itself is proportional to B. Then the Lorentz force and the experienced pressure is proportional to B^2 (Ref. [7]).

It is well known in EMF and other disciplines like magnetohydrodynamics (Ref. [13]) that this experienced pressure p actually equals the *energy density* of an oscillating or transient magnetic field parallel and in contact to a metallic surface:

$$p = \frac{1}{2} \cdot \frac{B^2}{\mu_0} \tag{5}$$

μ_0 represents the magnetic permeability of the vacuum. The energy density of a magnetic field is, therefore, also denoted as the *magnetic pressure p*. It readily manifests as an ordinary mechanical pressure (Ref. [13]), when exposing sufficiently conductive matter (i.e., the skin depth δ is small with respect to other geometries, compare Fig. 3) to a transient magnetic field. Interesting for acoustics, with just the known magnetic pressure p or the known magnetic flux density B in vicinity to a good conductor (metal with relatively small skin depth), a more detailed and complex determination of eddy currents and finally resulting Lorentz forces is not necessarily required. And, since most of the pressure is directed normally into the depth of the metal, a preferred excitation of longitudinal waves, propagating normally into the depth, can be expected. This is already described by previous workers, here cited from Ref. [5]: "the out-of-plane Lorentz force (into the depth) due to the dynamic field is about 10 times larger than the (lateral or radial) in-plane force." Only relatively small B field components are directed normally into the depth of the metal, basically located at the inner and the outer radius of the spiral coil. Here the field penetrates and then leaves the thin skin layer, and together with the annular eddy current some – relatively small – Lorentz forces in radial direction are generated.

At $B = 1$ Tesla the magnetic pressure is close to 400 kPa or 4 atmospheres (Eq. (5)) and this equals an energy density of 0.4 J per cm^3. In industrial EMF, an energy amount of about 15 kJ is converted into magnetic field energy. The magnetic energy, being proportional to B^2, is mainly (>70%) located and concentrated in the gap between coil and metal surface. Given that 10 kJ is homogeneously distributed in a volume of 100 cm^2 (here just taken as an example for the effective free space between coil and work piece in EMF applications), the mechanical pressure on the metal then would be 1000 atmospheres. This can rapidly deform a metallic work piece. That pressure is equivalent (Eq. (5)) to a magnetic flux density $B = 16$ T. In fact, even higher pressures are reported in EMF techniques.

It should be noted that the limiting problems in the EMF technique arise from the vast Lorentz forces acting on the coil windings rather than just heat due to the very strong current pulses. Furthermore, all known ferromagnetic materials are saturated above $B = 2$ T; thereby an iron or ferrite core will not significantly improve these techniques. The work is usually done with compact and rigid "copper alone" coils. As an interesting side remark, ferromagnetic iron will not be attracted by a strong magnetic induction field but it will be repelled, as all other non-magnetic metals.

The effective sound intensity I of an ultrasound wave at sound pressure p (peak value) in a material is

$$I = \frac{p^2}{2 \cdot Z_M} \tag{6}$$

with the characteristic acoustic impedance Z_M. At first sight, when implying a direct conversion of oscillating magnetic pressure into sound pressure, the excited sound intensity I should increase with B^4 or the stored energy E^2 (just by combining Eqs. (5) and (6)). This is a quadratic effect or an effect of second order. The relation directs the way towards non-contact and high intensity ultrasound generation via a "coil only transmitter": the ultrasound power should increase with the square of excitation power.

As an example, the magnetic pressure and the acoustic pressure at $B = 1$ T are given as 400 kPa (0.4 J/cm^3) and 200 kPa respectively. Only 200 kPa can be utilized for the acoustic pressure, because the full wave (peak to peak, from –200 to +200 kPa) must be within the magnetic amplitude of 400 kPa (see Fig. 2). The sound intensity I of a longitudinal bulk wave in aluminum ($Z_M \approx 17 \cdot 10^6$ Ns/m^3) then would be 1175 W/m^2 (Eq. (6)) or roughly 0.12 W/cm^2. At a given volume of 0.1 cm^3 for the magnetic energy (from spiral coil at 1 mm lift off gap g and 1 cm^2 footprint area A) and a frequency of 1 MHz the available power $P_{el,max}$ in the LC – circuit should be at least 40 mJ $\cdot \pi \cdot$ 1 MHz = 125 kW (from Eq. (3)). This accounts for the ideal case that all magnetic energy is exclusively and homogeneously allocated within the gap. Actually, only about 70% of the energy is in the gap (see the FEM discussion above) and secondly, the field is not exactly homogeneous in the gap but gradually weakened towards the metal target. This local inhomogeneity will, evaluating the FEM data in the gap and the B^2 dependence of the pressure, result in an additional 70% drop. Together these real effects account to a pressure reduction of approximately 50%. Then for 0.12 W ultrasound at 2 MHz in aluminum an available power of about 250 kW at 1 MHz should be present in the LC-circuit. Now a flux density of 1 T can be expected onto the metal. This suggests poor conversion efficiency and a vast mismatch situation; the vibrating metal surface can only convert about 0.5 ppm from the available power.

When applying a 100-fold higher electrical power density in the gap, i.e., an available power of 25 Megawatts at 1 MHz, the energy and the magnetic or acoustic pressure also increases 100-fold. As a result (Eq. (6)) a much more powerful ultrasound signal – now about 1.2 kW – is expected, corresponding to a magnetic flux of 10 T near the metal and a peak pressure of 40 MPa. Furthermore, the efficiency is improved significantly to 50 ppm, but is still not very good. To the benefit of this number, that available maximum power as a reference level is not identical to the actual power dissipation (which is considerably smaller) of the total system, and the local power dissipation in the metal is even much smaller.

It should be noted that this particular example (25 MW available power at 1 MHz, $g = 1$ mm and $A = 1$ cm^2, resulting into 40 MPa peak pressure) is – within reasonable accuracy – practically verified in the experiments below.

In a general formulation of the above considerations, the finally transmitted ultrasound power P_{US} of a ringing LC-circuit with released energy E, lift off g and coil area A over a metal with acoustic impedance Z_M can be stated as

$$P_{US} = \left(\frac{E}{g \cdot A} \cdot \frac{1}{2} \cdot \frac{1}{2}\right)^2 \cdot \left(\frac{1}{2 \cdot Z_M}\right) \cdot A \tag{7}$$

This formula should be fairly accurate for a situation, where g is about 1/10 of the coil's diameter (or the square root of the footprint area A), see FEM results in Fig. 3 and considerations above. And, on the other hand, the skin depth δ should be notably smaller than g. Inside the left bracket is the magnetic pressure, equivalent to the magnetic energy density: total energy E over active volume and then reduced to 50% by real effects, derived from FEM analysis. Another 50% reduction of the magnetic pressure is caused by the just 50% utilization of the only positive amplitude (Fig. 2) for bipolar acoustic amplitudes. Then the resulting acoustic pressure in the left bracket is squared and divided by 2 Z_M (the second bracket) and this is just the sound intensity according to Eq. (6). Actually, with a released energy of 8 J at $f = 1$ MHz, equal to an available power of 25 MW (Eq. (3)), and the geometries of $g = 1 \cdot 10^{-3}$ m and $A = 1 \cdot 10^{-4}$ m^2, in aluminum a momentary ultrasound power of 1175 W (equal to a momentary peak pressure of 40 MPa over 1 cm^2) is obtained from Eq. (7) and this was already discussed in the example above.

An efficiency η as the ratio $P_{US}/P_{el,max}$ can be readily derived from Eqs. (7) and (3):

$$\eta = \frac{P_{US}}{P_{el,max}} = \frac{1}{32} \cdot \frac{E}{Z_M \cdot A \cdot g^2 \cdot \pi \cdot f} \tag{8}$$

Eq. (8) can be altered by replacing the corrected energy density $E/(2 \cdot A \cdot g)$ by an energy density $B^2/2\mu_0$:

$$\eta = \frac{1}{32} \cdot \frac{B^2}{Z_M \cdot \mu_0 \cdot g \cdot \pi \cdot f} \tag{8b}$$

Eq. (8b) describes the efficiency as a function of the flux density B in vicinity to the metal. There are similarities to an expression reported much earlier by Dobbs (Ref. [14,15]):

$$\eta = \frac{P_{US}}{P_{RF}} = \frac{B_0^2}{Z_M \cdot \mu_0 \cdot \delta \cdot \pi \cdot f} \tag{9}$$

Despite the obvious similarity, the equation from Dobbs was derived in a quite different way, it has a somewhat different meaning and it applies for conventional EMATs with static field B_0.

When directly comparing Eqs. (8b) and (9), there appears a factor of 32 to the benefit of conventional EMATs. Another substantial difference to Eq. (8b) is that the skin depth δ appears instead of the lift off gap g. Since $\delta \ll g$ in relevant applications and together with the factor of 32, the efficiency of a conventional EMAT (Eq. (9)) seems to be very much higher than in the coil only concept from above (Eq. (8b)). This is however not the case, as briefly discussed now.

It must be noticed that in Eq. (9) just the *absorbed* power P_{RF} (Refs. [14,15]) is taken as the reference level for the ultrasound power P_{US}. Eq. (9), therefore, only addresses the *local conversion efficiency* within the test metal, with a somehow given field B_0 and a somehow inductively inserted net power P_{RF}. In contrast, Eqs. (8b), (8) offers a global description for the total setup, including the distant "coil only EMAT" and real attenuation effects over a distance g. And additionally, a much higher *available maximum* power in the LC-oscillation circuit is taken as the reference level for the conversion efficiency. The available maximum power in an oscillating LC-circuit even is considerably higher than the actual power dissipation (depending on τ, Eq. (4)) in the total system.

Particularly and to the benefit of coil only EMATs, the RF B-field cannot permeate into the depth of the metal; the field energy is concentrated close to and above the surface (Fig. 3), and this effect notably increases the energy density – equivalent to pressure. To the contrary, a static field B_0 from conventional EMAT will expand into the metal and this considerably dilutes the energy density B_0^2. For partial compensation the field source B_0 usually must be oversized, both in geometry (resulting in less compact designs) and total magnetic field energy. Therefore, the skin effect for an RF B-field should not be seen as a disadvantage but as an advantage. The skin effect helps to concentrate the B field in the region of interest. In particular, very high flux densities above 2 T (hardly possible for conventional EMATs) can be realized in the relatively smaller volume, see EMF and see the observation in Ref. [5] with the superior dynamic field. Additionally, the regions of high induction field automatically coincidence with the regions of high eddy currents. This is not necessarily the case for conventional EMATs with separated field generation.

In another substantial difference to normal EMATs the coil only concept will – since only positive pressures result (Fig. 2) – transfer a linear momentum ("LM") to the metallic test object. The test object will be repelled by the inductor and this is the intentional purpose in EMF technologies. A linear momentum can be easily determined by measuring the (constant) velocity of a mass, after momentum transfer by the coil. The linear momentum LM is delivered within a few periods of the MHz oscillation, Fig. 2 suggests the completion of the process after a few μs.

Since in Fig. 2 the maximum pressure p (and also the maximum force F) is normalized to "1 N/m^2" or "1 N" for the damped oscillation with $f = 1$ MHz and $\tau = 3$ μs, the normalized linear momentum ("NLM") from this magnetic pressure oscillation is

$$NLM = \int_0^\infty F(t)dt = \int_0^\infty 1N \cdot \sin^2(2\pi ft) \cdot e^{\frac{-2(t-\frac{1}{4f})}{\tau}} dt \approx 0.88 \cdot 10^{-6}\,\mathrm{kg}\,\frac{\mathrm{m}}{\mathrm{s}} \tag{10}$$

For an experimental high power oscillation with frequency f and decay time τ – which both are easily observable with a standard oscilloscope – the real linear momentum LM of the repelled test object can be set in relation to the normalized momentum NLM. The ratio of real LM to NLM equals the ratio of real maximum force F_{max} to 1 N. For 1 MHz and $\tau = 3$ μs:

$$\frac{F_{max}}{1N} = \frac{LM}{0.88 \cdot 10^{-6}\ \mathrm{kg}\ \frac{\mathrm{m}}{\mathrm{s}}} \tag{11a}$$

In more general, for any other frequencies f and other decay times τ of a pulsed LC-discharge:

$$F_{max} = \frac{LM}{\int_0^\infty \sin^2(2\pi ft) \cdot e^{\frac{-2(t-\frac{1}{4f})}{\tau}} dt} \tag{11b}$$

Quantitative information about F_{max} is very welcome, since hereby also the practical and maximum magnetic pressure p_{max} is reasonably accessible via the affected area A. Obviously, p_{max} is tied to the achieved sound pressure in the metal.

p_{max} can be compared with the total energy E in the system (stored in the capacitor C before switching), in best case it should equal the energy density in the gap g with area A. In practical setups and as discussed above, with a distance g ≈ 1/10 ·square root (A), the energy density close to the metal is expected to be only 50% of the best case limit $E/g \cdot A$.

2. Techniques, equipment and experimental setup

50 high voltage (40 kV max) and 3 nF ceramic pulse capacitors (Murata DHS N4700) were combined in parallel to 150 nF. Such ceramic capacitors are commonly used e.g. in pulsed excimer lasers (Ref. [16]), where the stored energy must be delivered within some tens of nanoseconds and, consequently, at power levels of many Megawatts and currents in the kA range. These pulse capacitors obtain low internal inductance and resistance and they are proven to deliver many millions of pulses over their lifetime without fatigue or failure.

The multiple capacitors were interconnected with a low inductance wiring (short and wide strips). At an experimental charge

voltage of 15 kV the stored energy E is close to 17 J (Eq. (1)). A standard high voltage DC supply with an adjustable current up to 20 mA and adjustable voltage up to 30 kV was used as a charge supply for the 150 nF. It is connected over a high voltage resistor (500 Ω) for decoupling the pulsed power from the DC supply.

For a desired oscillation frequency of 1 MHz, a total inductance L_T = 170 nH (including the parasitic inductance L_P from all wiring, switch, capacitor) is required (Eq. (2)). The spiral coil L_I, therefore, must be less than 170 nH. Since the stored energy E in capacitor bank C is converted to a major portion into magnetic field energy $E = L/2 \cdot I^2$ (Eq. (1b)) the maximum discharge current after closing the switch should then be close to 14 kA. The characteristic electrical impedance Z_{el} of such L-C-oscillation circuit is then 15 kV/14 kA ≈ 1 Ω (or alternatively by Eq. (2)). All real resistance in the LC-circuit must be held significantly below 1 Ω for an oscillation without excessive attenuation: Eq. (4), $\tau = L/R > 3$ µs, better: $\tau > 4$ µs. The available maximum power (Eq. (3)) is then close to 52 MW at stored energy E = 17 J.

Not all power or magnetic energy is present in the spiral coil L_I, because the energy is proportionally divided to the all serial inductances $L_T = L_I + L_P$ in the system. Without spiral coil L_I (shortcut) and from parasitic L_P only, the observed oscillation (or resonance) frequency of the system is 1.43 MHz, and (Eq. (2)) $L_P \approx 83$ nH. In consequence, L_I must be 85–90 nH to meet the 1 MHz and only about 50% of the total energy or available power is present in the flat spiral coil, about 8 J. Then it can be reasonably estimated that only about 25 MW or less can be provided from the spiral coil. Without load (not coupled to metal target), a $\tau \approx 4$ µs is observable. Therefore all resistances in the system (switch closed) add up to less than 0.1 Ω.

The high power oscillation event can be readily observed from a distance of about 20 cm with a single loop of copper wire. The diameter is about 5 cm and the loop is loaded with a very low inductance 0.2 Ω resistor (i.e., a bundle of many resistors in parallel). The voltage over the 0.2 Ω is proportional to the current in the loop and can be readily observed via standard coax cable with a standard oscilloscope. Actually, the current in the loop is predominantly an eddy current from the distant LC-pulse generator, and it resembles the discharge current in the LC-circuit itself. With the observed oscillation and attenuation, a reasonable estimation of f and τ is possible. Due to the high momentary power no extra amplifier is needed, the signal from the loop (several Volts) is well suited for a standard oscilloscope. It must be noted that definitely an inductive signal is detected and not any other EMI effect: the magnetic coupling of the loop can be readily verified by just twisting the loop by 90° (plane then parallel to B). The signal then vanishes.

An important element for the pulsed LC-circuit (Fig. 1) is the switch. Required properties are low inductance (≪150 nH), low resistivity (≪1 Ω) and the capability to bear 15 kA and to withstand 15 kV. Furthermore, the switch must tolerate positive and negative currents during the oscillation and it must transit from high impedance (≫1 MΩ) to low impedance (≪1 Ω) within a time much smaller than 1 µs.

The requirements can be matched with commercially available thyratron tubes. Nowadays even an all-solid-state switching is established for similar applications, partly combined with magnetic pulse compression (compression in time). These all-solid-state techniques are maintenance free and have demonstrated a practically unlimited lifetime (Ref. [16]).

In our experiments, for the sake of simplicity and flexibility, a low inductance spark gap with sound absorber was applied, simply working in air. The switching time of such spark gap after ignition is much shorter than 1 µs (can be few nanoseconds) (Ref. [17]) and all requirements above (15 kV, 15 kA, ≪1 Ω after ignition) are well fulfilled. A certain amount of energy is consumed for the formation of very conductive and highly ionized plasma in the spark gap; this energy (estimated <5 J) is taken from the initial energy in the capacitor. For high power and "coil only" ultrasound generation a similar circuitry with a triggered spark gap was already presented in Ref. [7], although discussed only for smaller ultrasound frequencies (100 kHz…) and – together with a copper foil very close to the coil – intended as a mechanically contacting transducer for applications on (non-metallic) concrete. The basic disadvantage of such old-fashioned high power switch is the burn-off behavior after several hundred shots, requiring frequent maintenance. A silencer is mandatory: the plasma flashes emit considerable noise, naturally including ultrasound.

Therefore it is also interesting to compare the ultrasound pulses from a "coil only EMAT" with the impact of 17 J sparks itself from the capacitor bank. The sparks can be directly released onto the surface of the metallic test sample. Although representing a non-contact method over a certain distance (about 9 mm gap from electrode to surface), such spark technique cannot be called non-destructive. Considerable scorch marks affect the surface, and this cannot be tolerated in every application.

Additionally, a comparison with laser induced ultrasound is carried out (Refs. [18–20]), from a pulsed Nd:YAG laser (Quantel Ultra 100) emitting at 1064 nm and 532 nm.

The laser pulse delivers 20 mJ energy within 8 ns and it is focused onto a small spot (<1 mm^2) of the test metal. As with the spark, the method is non-contact but however not "non-destructive": breakdown plasmas and impact marks affect the surface. These micro-explosions on the surface are apparently required for noteworthy ultrasound signals.

The flat spiral coils itself were made from standard PCB material with an extra thick copper layer (120 µm) or are, alternatively, manually wound spirals from regular copper wire. These spiral coils with a diameter of 25 mm down to 10 mm consist of just a few windings (<10) to meet the <170 nH requirement for f = 1 MHz. Due to the skin effect at 1 MHz in copper, the conducting material is not needed to be much thicker than 0.2 mm. In the pulsed power application the coils are exposed to high mechanical, thermal and electrical stress. The spiral coils were immersed in epoxy resin to mechanically stabilize and to electrically insulate the windings, since already two neighbored windings (=1 turn) must withstand a RF voltage difference of about 1000 V. Practically even more delicate is the voltage difference towards the test metal. Since an air gap (=the lift of distance g) of even almost 1 cm is overcome by the 15 kV, the surface area of the spiral coil is insulated by a 200 µm polymer foil (similar to Polyimide), laminated onto the coil with epoxy resin. With these insulating layers onto the surface, a gap g to a test metal of at least 0.5 mm is defined. An imperfection in the insulation – this already can be a small air inclusion – regularly results in instantaneous failure of the coil within one power pulse. On the other hand, a well handcrafted coil withstands a virtually unlimited number of shots.

Interestingly, the mechanical and thermal stability of the coils appears to be less delicate. The µs short and intensive mechanical forces can apparently be taken by the inertial mass of the high density copper material. Thermal problems become an issue at high repetition frequencies. At low repetition rates of about 1 Hz, a conventional air blower is sufficient for cooling a free standing coil. For higher repetition frequencies (10 Hz…) the back of the spiral coil was laminated onto a ceramic boron nitride block. This material is both a good electrical insulator and a good thermal conductor, thereby acting as a heat sink for the relatively small coil.

An aluminum rod with 30 mm diameter and 0.89 m length served as metallic test material, Fig. 4. The two end faces are plane. One face is exposed to a non-contact ultrasound generator, i. e., a coil only EMAT or the 17 J spark impact or the laser pulse. The other face was equipped with a ceramic PZT disk (10 mm diameter,

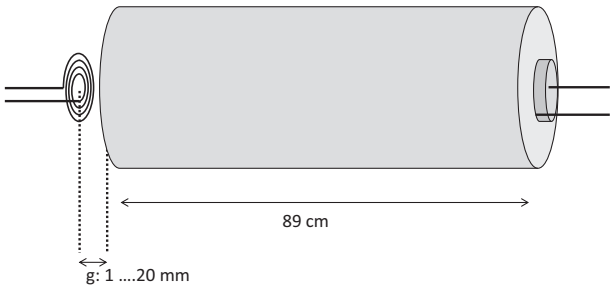

Fig. 4. Experimental setup. The spiral coil transmitter is positioned in a distance g to an aluminum rod. The other end of the rod is equipped with a piezo crystal and detects ultrasound events with a 140 μs delay from the 89 cm rod.

1 mm thickness), this piezo crystal was attached onto the aluminum face with paraffin wax. The two contacts of the piezo were loaded with 100 Ω and a parallel inductor of 3 μH for a prefered selection of 2 MHz and at 700 kHz bandwidth. This detector was directly connected to a standard oscilloscope; no extra signal amplifier was involved here.

An ultrasound shot into the rod́s ending should result in a piezo signal at the other side after the characteristic runtime along 89 cm in aluminum: 0.89 m/6350 ms^{-1} ≈ 140 μs. The delay time of 140 μs is well suited to distinguish strong electromagnetic interference (EMI) from a real ultrasound signal in the aluminum. The aluminum rod works as a waveguide and it actually disperses the ultrasound into several modes of longitudinal propagation. The investigation of this mode dispersion is however not within the scope of this contribution, see instead Ref. [21].

Furthermore, 30 × 30 mm platelets from aluminum, ferromagnetic steel with and without zinc coating and stainless steel (non-ferromagnetic) were prepared. These metal chips were placed, in a horizontal setup, onto the spiral coils. Within a magnetic pulse, a metal chip receives a linear momentum LM (Eqs. (10) and 15) and jumps against earth's gravity to a certain height h. This height h is readily observable with sufficient accuracy (only applies in square root of Eq. (16)), even with the naked eye. It must be noted, that an insulating material (e.g., a glass plate) does not jump. The LM is actually provided by the electromagnetic pressure and not by any mechanical vibration. The LM of the metal chip is

$$LM = m \cdot \sqrt{2 \cdot G \cdot h} \tag{12}$$

with m = mass of the metal chip, gravity G = 9.81 m/s^2, h = achieved height. With the known LM the maximum force F_{max} (Eq. (11b)) is derived, and then together with the inductive footprint area A, a characteristic magnetic pressure is accessible.

3. Experimental results

In Fig. 5 the oscilloscope screenshots from an 8 J pulse (i. e., a total 17 J energy in the system, including the parasitic inductances) through a spiral coil with approximately 1 cm^2 footprint A and 1 mm gap g to the aluminum rod are displayed. Channel 1 displays the piezo signal and channel 2 (also used for triggering) represents the induction signal in the wire loop.

In Fig. 5a clear piezo signal after 140 μs and with 15 V amplitude is present. In this moment, the piezo delivers more than 2 W of electrical power into the 100 Ω load. Note that the piezo covers only 10% of the rods face and it is not well coupled (just a paraffin wax layer with unintentional air inclusions) to the aluminum. Unquestionably the piezo detects a considerable ultrasound signal at the expected delay time. Even a multiple echo (distance then 280 μs, several times travelling forth and back over 180 cm) is observable, but not shown here. The discrete replicas in the ultrasound signal after 140 μs and at a characteristic distance of about 10 μs originate from different propagation modes (Ref. [21]) in the 30 mm rod, which also shall not be further discussed here.

Fig. 5b zooms into the electromagnetic excitation at t = 0 μs. A damped oscillation at 1 MHz is present in channel 1, the decay time τ resembles Fig. 2, and the amplitude halves every 2 μs. Therefore, τ can be reasonably estimated to be 3 μs here.

Fig. 5c zooms into the piezo signal after 140 μs. The predominant frequency is close to 2 MHz. The effective duration of a received ultrasound pulse signal (within a certain propagation mode) is 2–3 μs. The actual duration is assumed to be even shorter, since the piezo detector itself exhibits some time constant or limited bandwidth.

When comparing the above ultrasound intensity (using the exact same piezo detector) with those signals from a direct 17 J spark impact into the aluminum rod or a nanoseconds laser impact, the electromagnetic method outperforms the other methods by far: the spark signal shows a very similar pattern in time after 140 μs (Fig. 5a) but achieves only 0.5 V amplitude and the laser pulse induced ultrasound (including plasma and resulting point defect on the aluminum surface) is just close to 0.03 V.

The electromagnetic induced ultrasound intensity I at 2 MHz and in W/cm^2 is, therefore, almost 1000 times stronger than from the direct spark impact with even doubled energy (17 J) and 250,000 times stronger than from the laser shot.

To better quantify the ultrasound intensities and pressures, 1 MHz electromagnetic "jump" experiments were made, here again with about 8 J energy in the transducer coil. Table 1 represents the data:

Experimental uncertainties exist with the experimental momentum LM (particularly the smallest jump from the stainless steel is not very accurate), with the characteristic decay time of the oscillation τ and with the actually affected area A. Nevertheless, a virtual independence of the experienced pressures from the metal type is obtained. The magnetic pressure implies a magnetic field of $B \approx 10.5$ T and a magnetic energy density of ≈4 J/0.1 cm^3 close to the metal. Actually, a total magnetic energy of about 8 J or an available power of 25 MW was present in the coil. The experimentally observed reduction of magnetic energy density down to only 50% close to the metal is in well accordance to the above considerations from the FEM model and the herein computed distribution of field energy. Furthermore, the jump data is – within the limited experimental accuracy of such delicate high voltage experiments – in quite reasonable accordance to the discussed example above, with the presumed 10 T and the equivalent 40 MPa.

Fig. 6 reveals the ultrasound amplitude at 2 MHz as a function of capacitor charge voltage (Eq. (1)) and at fixed geometry. The charge voltage ("k**V**") proportionally converts into flux density of the spiral coil ("**V** s/m^2") and the ultrasound power – as discussed in the introduction – should increase with B^4 and the sound pressure p with B^2. The piezo signal is proportional to the sound pressure or amplitude, and therefore, the piezo signal should increase with the square of the capacitor charge voltage. A parabola is expected and apparently, this is quite well matched. Also at 16 kV charge, a piezo signal of almost exactly 16 V is obtained (this value not included in the graph for better representation of the smaller values).

Fig. 7 shows the electromagnetically induced 2 MHz ultrasound after 140 μs as a function of "lift off distance" g for two different spiral coils. One coil has an effective diameter of 3 cm, the other 1.4 cm. The area A of the circles is respectively 7 cm^2 and 1.5 cm^2. These areas just can be counted for approximately 2/3, due to the inner bore in the spiral coil. The corrected A for the coils is then about 5 cm^2 and 1 cm^2.

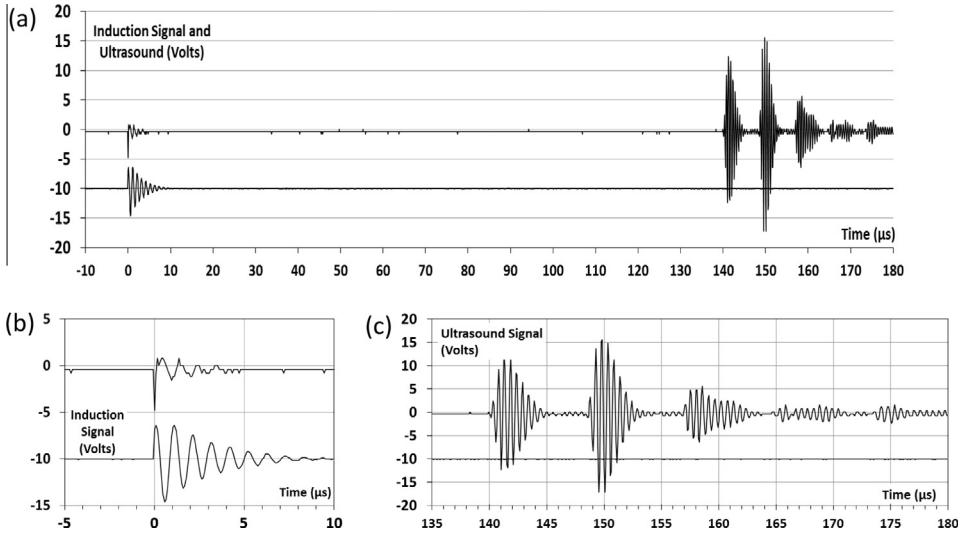

Fig. 5. Ultrasound signals (upper line) and induction signals (lower line) from a multi MW induction pulse at 1 MHz. Signal amplifiers are not required. At 0 µs the induction pulse and after 140 µs a strong ultrasound signal appears, separated in discrete propagation modes through the aluminum rod. In (b) the induction pulse. Besides an EMI affected first half wave, a regularly damped 1 MHz oscillation with $\tau \approx 3$ µs appears. The ultrasound signal in (c) obtains strong 2 MHz components.

Table 1
Electromagnetic jump experiments against earth's gravity. Different metal chips are vertically repelled to a certain height h by a spiral coil with $A \approx 1$ cm^2 and $g \approx 1$ mm. The coil is excited with 2–3 µs short pulses at 1 MHz and 8 J energy, equivalent to 25 MW available power. Momentary pressures of about 40 MPa act on the metal chips, equivalent to a flux density of about 10 T.

Material and Size of the metal chip	Aluminum $30 \times 30 \times 1$ mm^3	Ferromagnetic steel $30 \times 30 \times 0.55$ mm^3	Stainless steel non-ferromagnetic $30 \times 30 \times 1$ mm^3
Mass of the chip	$2.43 \cdot 10^{-3}$ kg	$3.91 \cdot 10^{-3}$ kg	$7.08 \cdot 10^{-3}$ kg
Jump height h	0.13 m	0.03 m	0.008 m
Experimentally observed Linear Momentum LM (Eq. (12))	$3.9 \cdot 10^{-3}$ Ns	$3.0 \cdot 10^{-3}$ Ns	$2.8 \cdot 10^{-3}$ Ns
Normalized linear momentum (NLM) (Eq. (10))	$\tau \approx 3$ µs $8.8 \cdot 10^{-7}$ Ns	$\tau \approx 2$ µs $6.4 \cdot 10^{-7}$ Ns	$\tau \approx 2$ µs $6.4 \cdot 10^{-7}$ Ns
Maximum force F_{max} (Eq. (11b))	4430 N	4700 N	4370 N
Maximum magnetic pressure p_{max} ($A \approx 1$ cm^2)	$44 \cdot 10^6$ Pa ≈440 Atmospheres	$47 \cdot 10^6$ Pa ≈470 Atmospheres	$44 \cdot 10^6$ Pa ≈440 Atmospheres
Maximum acoustic pressure at 2 MHz	$22 \cdot 10^6$ Pa	$23 \cdot 10^6$ Pa	$22 \cdot 10^6$ Pa
Momentary acoustic intensity at 2 MHz (Eq. (6))	1.4 kW/cm^2	0.6 kW/cm^2	0.55 kW/cm^2

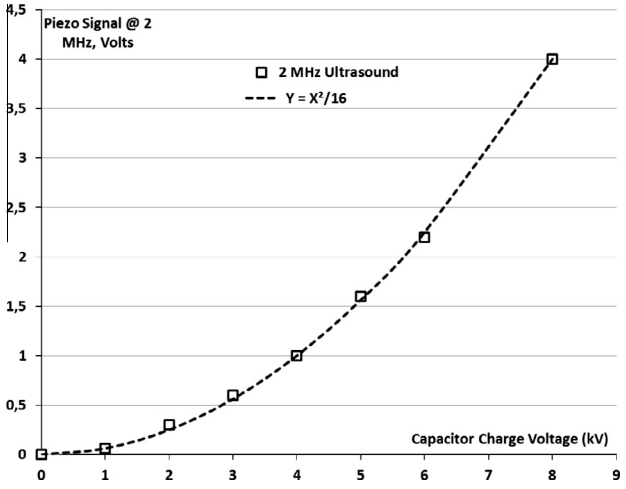

Fig. 6. Piezo amplitude at 2 MHz as a function of capacitor charge voltage. The observed data direct to a second order (quadratic) relation. Here for comparison a simple parabola $y = x^2/16$, dashed line. Actually, also at 16 kV charge a signal close to 16 V results. This is not shown here for better representation of the smaller values.

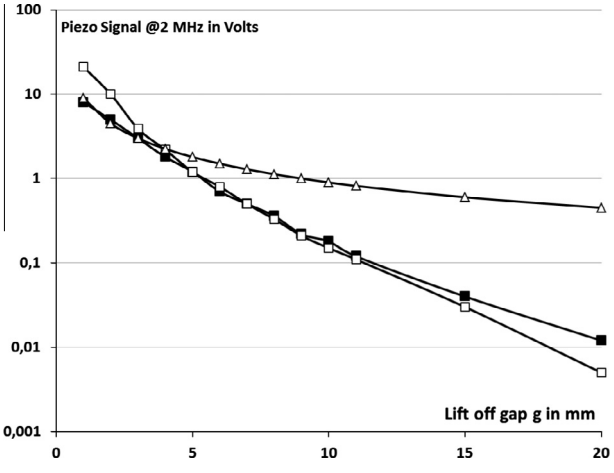

Fig. 7. Piezo amplitude at 2 MHz for a 1 cm^2 (white squares) and a 5 cm^2 coil (black squares) at constant energy and as a function of distance g. Towards increasing g the smaller coil is more affected. On the other hand, at small distances the smaller coil is more effective. For comparison, the functionality of Eq. (8) is displayed (Ultrasound Intensity $\sim 1/g^2$, white triangles). At relatively low distances g the real behavior can be fairly matched.

At the same total energies, the ultrasound intensity and conversion efficiency is significantly higher for the smaller coil at $g = 1$ mm, following Eqs. (7) and (8) with the suggestion of the power density as a relevant parameter for efficient electroacoustic coupling.

With increasing gap g the ultrasound intensity rapidly decreases, almost exponentially. The smaller coil is affected more by the distance, so that above $g = 1$ cm the wider coil becomes superior. Actually the magnetic field energy is more localized around a smaller coil, all gradients are higher. In consequence, the magnetic pressure $\sim B^2$ of a small coil is more affected by distance than for a wider coil.

It must be noted that for higher distances g the B field becomes quite inhomogeneous in the gap, it gradually localizes towards the coil (Fig. 3b). Additionally the affected footprint area A will increase. Therefore a simple calculation of the behavior with Eq. (7) will not match for higher distances; the actual situation then becomes more disadvantageous. However at small distances (1–3 mm) and for the 5 cm^2 coil, the simplified relation from Eq. (7) seems to fairly match the experimental observations.

4. Discussion and conclusion

The experimental findings, although not obtained in utmost accuracy due to the quite delicate handling with an open high voltage capacitor with considerable pulsed power capability, apparently support the key considerations of this contribution.

The jump experiment comes close to the example from the introduction, where from a 25 MW available power at 1 MHz a sound intensity I or power ($A = 1$ cm^2) of 1.25 kW at 2 MHz was predicted for aluminum, equivalent to 40 MPa peak pressure. In the experiments, the power offering was about 25 MW at 1 MHz and resulted to nominally 44 MPa peak pressure. The difference is – as we believe – reasonably small within the accuracy of all experimental uncertainties and approximations.

A noteworthy observation is the virtual constancy of maximum pressures p_{max}, independent from the metallic target material. This result, originating from similar eddy currents in even quite different metals, supports the general concept of magnetic pressure also for ultrasound. The more pronounced losses in steel or stainless steel due to higher skin resistance just result in more attenuation of the oscillation. Not the intensity but the pulse duration τ should become smaller. As an additional remark here, the nominal skin depth in stainless steel ($\approx$400 μm at 1 MHz) is not very small with respect to the applied gap of 1 mm. But nevertheless, the observed momentum in stainless steel was in the expected range and this supports the general idea. The influence of a relative thick skin depth should be investigated more precisely in subsequent investigations. Nevertheless, the method appears to be suitable for all metal types.

The parabolic behavior of piezo output voltage as a function of capacitor charge voltage (Fig. 6) is in good accordance with Eqs. (7) and (8) and other considerations in the introduction: ultrasound power $\sim$ (electromagnetic power)^2. An effect of second order or quadratic behavior is present. Higher power levels should further increase efficiency and then resulting in much higher ultrasound intensities. Even just an increased *power density* can considerably improve the efficiency of the ultrasound transmission. It appears from Fig. 7 that for small lift off gaps (g: <10 mm) the smaller spiral coil with 1 cm^2 is clearly superior for high intensity ultrasound. A small and quite powerful NDT transducer might be attractive for certain applications.

The internal inductances of the pulse generator must be held smaller than the inductive transducer for good power utilization (non-linear effect of electro-acoustic conversion!). The realization of higher frequencies towards 10 MHz probably requires smaller capacitors with smallest parasitic inductance. High energy content then must be achieved with even higher charge voltages.

For higher distances (cm) the geometries of the coil must be larger for better coupling. The achievable intensities however still strongly decline over distance.

The presented technique in the current state preferably transmits longitudinal waves and additionally, it cannot readily detect ultrasound. Ultrasound detection, therefore, must be realized by a separate and additional device and this could be a conventional EMAT or an optical receiver. Alternatively, the presented "coil only" transmitter can be equipped with an additional permanent magnet (only resulting in fields of typically < 1 T, Ref. [5]) and it then operates as a conventional EMAT for detection purposes. Another alternative would be the superimposition of a strong and short RF burst at relatively high frequencies (say 10 MHz) to the coil, at a time where the ultrasound echo is expected from target. An RF generator at quite different frequency (10 MHz) can be well decoupled from the 1 MHz pulsed power. The echo (2 MHz) mixes with the 10 MHz excitation (eddy currents at 10 MHz) and results into a 8 and 12 MHz electrical signal in the coil. The 12 MHz echo then could be separated and analyzed. As with a static field of conventional EMAT, the 10 MHz excitation should be strong for a better 12 MHz echo signal. But in contrast to a conventional EMAT, the 10 MHz field would be – again – concentrated by the skin effect and additionally it spatially well coincidences with the eddy current in the metal. And additionally, it preferably would detect longitudinal waves.

As another unsolved technical problem here, the small coil only transducer is not supplied over a flexible cable but directly connected to the relatively large pulse generator. The transmission of short pulses with many kA through a compact and flexible cable towards a small transmitter is certainly much more attractive for practical applications. This appears quite challenging and should be investigated in future work.

Acknowledgement

This work is initiated and supported by the internal research founding of the University of Applied Sciences Ruhr-West.

References

[1] H.M. Frost, Electromagnetic-ultrasonic transducers: principles, practice and applications, in: W.P. Mason, E.N. Thurston (Eds.), Physical Acoustics, vol. XIV, Academic Press, New York, USA, 1979, p. 179.
[2] R.B. Thompson, Physical principles of measurements with emat transducers, in: W.P. Mason, R.N. Thurston (Eds.), Physical Acoustics, vol. XIX, Academic Press, New York, 1990, pp. 157–200.
[3] B.W. Maxfield, C.M. Fortunko, The design and use of electromagnetic acoustic wave transducers (emats), Mater. Eval. 41 (1983) 1399–1408.
[4] W.P. Mason, R.N. Thurston, Physical Acoustics, Electromagnetic—Ultrasound Transducers: Principles, Practice and Applications, vol. XIV, Academic Press, New York, NY, 1970.
[5] X. Jian, S. Dixon, R.S. Edwards, Modelling ultrasonic generation for Lorentz force EMATs, Insight (BINDT) 46 (11) (2004) 671–673.
[6] X. Jian, S. Dixon, R.S. Edwards, J. Morrison, Coupling mechanism of an EMAT, Ultrasonics 44 (2006) e653–e656.
[7] Josef Krautkrämer, Herbert Krautkrämer, Ultrasonic testing of materials, 4th fully rev. ed. Springer-Verlag, Berlin, New York, 1990. ISBN 3-540-51231-4.
[8] G. Harvey, D.E. Brower, Metal Forming Device and Method, U.S. Patent Documents 2,976,907, General Dynamics Corporation, 28.08.1958.
[9] B.P. Leftheris, Method of Welding Metals Using Stress Waves, U.S. Patent Documents 3,961,739, Grumman Aerospace Corporation, 07.05.1974.
[10] R. Weadock, Magnetic Forming Apparatus, U.S. Patent Documents 3,348,397, General Motors Corporation, 22.10.1964.
[11] Journal of Materials Processing Technology, vol. 211, Issue 5, Special Issue: Impulse Forming, in: A. Erman Tekkaya, Julian M. Allwood (Eds.) Electromagnetic Forming—A review, 1 May 2011, pp. 787–829.
[12] See e.g. Wikipedia.org "skin effect" or standard text book electrodynamics.
[13] See e.g. Wikipedia.org "magnetic pressure" or standard text book electrodynamics.

[14] E.R. Dobbs, Electromagnetic generation of ultrasonic waves, in: W.P. Mason, R.N. Thurston (Eds.), Physical Acoustics, vol. X, Academic Press, New York, 1973, pp. 127–189.
[15] E.R. Dobbs, J.D. Llewellyn, Non-destruct, Test 4 (1971) 49–56.
[16] D. Basting, G. Marowsky, Excimer Laser Technology, Springer, 05.12.2005, ISBN: 3-540-20056-8.
[17] E.E. Kunhardt, The formation of pulsed discharges, Proc. Fourth IEEE Pulsed Power Conf. (1983) 206–211.
[18] C.B. Scruby, Some applications of laser ultrasound, Ultrasonics 27 (1989) 195–209.
[19] C.B. Scruby, R.J. Dewhurst, D.A. Hutchins, S.B. Palmer, Research Techniques in Non-destructive Testing, vol. 5, in: R.S. Sharpe (Ed.), Academic Press, London, UK, 1982, p. 281.
[20] R.D. Huber, R.E. Green Jr., Non-contact acousto ultrasonics using laser generation and laser interferometric detection, Mater. Eval. 49 (1991) 613–618.
[21] J.R. Hutchinson, C.M. Percival, Higher modes of longitudinal wave propagation in thin rods, J. Acoust. Soc. Amer. 44 (5) (1968) 1204–1210.